Drug Design, Development and Therapy

Dovepress

open access to scientific and medical research

Open Access Full Text Article

ORIGINAL RESEARCH

A Novel Folic Acid Receptor-Targeted Drug Delivery System Based on Curcumin-Loaded β-Cyclodextrin Nanoparticles for Cancer Treatment

Weiyong Hong[1,2,*]
Fangyuan Guo[2,*]
Nan Yu[2]
Sanjun Ying[2]
Bang Lou[2]
Jiangqing Wu[2]
Ying Gao[2]
Xugang Ji[2]
Haiying Wang[1]
Aiqin Li[3]
Guoping Wang[4]
Gensheng Yang[2]

[1]Department of Pharmacy, Taizhou Municipal Hospital, Taizhou, 318000, People's Republic of China; [2]College of Pharmaceutical Science, Zhejiang University of Technology, Hangzhou, 310014, People's Republic of China; [3]Zhejiang Share Bio-Pharm Co., Ltd, Hangzhou, 310019, People's Republic of China; [4]Zhejiang Dayang Biotech Group Co., Ltd, Hangzhou, 311616, People's Republic of China

*These authors contributed equally to this work

Correspondence: Gensheng Yang
College of Pharmaceutical Science, Zhejiang University of Technology, Hangzhou, 310014, People's Republic of China
Tel +86571-88871077
Fax +86571-88320913
Email yanggs@zjut.edu.cn

Purpose: A novel folate receptor-targeted β-cyclodextrin (β-CD) drug delivery vehicle was constructed to improve the bioavailability, biosafety, and drug loading capacity of curcumin. Controlled release and targeted delivery was achieved by modifying the nanoparticles with folic acid (FA).

Methods: Folate-conjugated β-CD-polycaprolactone block copolymers were synthesized and characterized. Curcumin-loaded nanoparticles (FA-Cur-NPs) were structured by self-assembly. The physicochemical properties, stability, release behavior and tumor-targeting ability of the fabricated nanoparticles were studied.

Results: The average particle size and drug loading of FA-Cur-NPs was 151.8 nm and 20.27%, respectively. Moreover, the FA-Cur-NPs exhibited good stability in vitro for 72 h. The drug release profiles showed that curcumin from FA-Cur-NPs was released significantly faster in a pH 6.4 phosphate buffered solution (PBS) than in pH 7.4, indicating that curcumin can be enriched around the tumor site compared with normal cells. Additionally, the internalization of FA-Cur-NPs was aided by FA receptor-mediated endocytosis, and its cytotoxicity was proportional to the cellular uptake efficiency. Furthermore, in vivo studies confirmed that FA-Cur-NPs exhibited marked accumulation in the tumor site and excellent antitumor activity.

Conclusion: These findings suggest that FA-Cur-NPs are a promising approach for improving cancer therapy through active targeting and controllable release.

Keywords: curcumin, β-CD-polycaprolactone copolymers, folate receptor, targeted drug delivery, HeLa cells

Introduction

Cancer is the most fatal disease threatening human health. According to GLOBOCAN estimates, there were approximately 19.3 million new cases and almost 10.0 million deaths in 2020.[1] Current therapeutic approaches developed for cancer treatment include chemotherapy, immunotherapy, radiation therapy, and surgical excision;[2–4] among them, chemotherapy is the most effective and inexpensive treatment.[5] However, poor targeting selectivity is the main drawback of traditional drugs, which usually cannot distinguish tumors from normal tissues.[6] Therefore, a high dose is administered, resulting in serious adverse effects (eg, side effects and multidrug resistance).[7] Curcumin exhibits a wide range of pharmacological activities such as anti-inflammation, antioxidant, antimicrobial, and anticancer.[8–10] Moreover, the anticancer activity with a high safe dose[11] and ability

of multiple cell signaling pathways to regulate different tumors, such as breast, cervical, stomach, liver, and pancreatic cancers as well as colon and epithelial cell carcinomas have received the most attention.[12–15] However, the low water solubility, rapid decomposition, and lack of specific targeting of curcumin under physiological conditions limited its clinical application.[16]

To overcome these barriers, nanotechnology has been applied for drug delivery,[17] and active targeted delivery through tumor microenvironment-stimuli responsive systems, such as pH-responsive,[18,19] redox-sensitive,[20] and targeting molecule-conjugated nanocarriers,[21] has been employed for tumor diagnosis and treatment. Targeting molecule-conjugated nanocarriers have been widely investigated due to their excellent selectivity. Folic acid receptors are a promising antitumor target as they are overexpressed on the surface of 40% of solid tumors,[22,23] but negligible in the majority of healthy tissues.[24] Folate-drug delivery systems can enter tumor cells through receptor-mediated endocytosis and avoid non-specific effects on normal tissues. Meanwhile, cellular uptake by target cells increased and the therapeutic agents were transferred to tumor cells.[25] β-cyclodextrin (β-CD) is cyclic oligosaccharides that possess a hydrophilic external surface and a hydrophobic internal cavity and has become a research hotspot due to its moderate lumen size, high drug loading, low production cost, improved lipophilic drug stability, easy modification by molecules, and good toxicological characteristics.[26,27] Recently, nanocarriers based on β-CD have been employed to improve drug bioavailability. Popat et al[28] studied the therapeutic effect of curcumin-loaded cyclodextrin chitosan nanoparticles (CUR-CD-CS) on a skin cancer cell line (SCC25) and found that cyclodextrin not only increased the solubility of curcumin but also promoted its cellular uptake. Hyun et al[29] prepared a new targeting nanoparticle (CDPF) consisting of folic acid (FA), β-CD, and polyethylene glycol (PEG) to improve doxorubicin targeting for breast cancer. However, these nanoparticles exhibited uncontrollable drug release (ie, fast drug release rate and few differences in the drug release rate between tumor areas and normal cells). These drawbacks may be overcome by modification the hydrophilic/lipophilic properties of the drug-carrying polymers. In addition, the drug loading of the previously studied nanoparticle is less than 10% due to the large molecular weight of the carrier materials.[7] In order to ensure a sufficient drug dosing so as to guarantee an adequate therapeutic effect, it is undesirably necessary to include a large number of non-therapeutic carrier materials, which would enter the body during the drug administration and potentially cause side effects. Therefore, improving the drug loading and reducing even eliminating the overuse of such carrier materials is a critical task that needs to be nicely accomplished.

In view of this, we attempted to develop a nano-drug system consisting of FA, β-CD, and ε-caprolactone (ε-CL) for improved curcumin delivery to cervical cancer tissues, which overexpress folic receptors (FRs), to achieve controllable release in vitro and in vivo. In this system, FA was used as a targeting molecule to specifically bind to FRs. β-CD, the main skeleton for drug encapsulation, was modified by ε-CL and FA to adjust the hydrophilic/lipophilic properties for controlling drug release and achieving target delivery in tumors, respectively. Curcumin was selected as a model drug to limit multidrug resistance after administration. The FR-targeting, curcumin-loaded, β-CD-based nanoparticles (FA-Cur-NPs) were prepared by self-assembly using a solvent volatilization method. Thanks to the cyclic structure of β-CD, the drug loading efficiency of the nanoparticles was remarkably improved. Thereafter, the pharmacokinetics and pharmacodynamics of FA-Cur-NPs were further studied to evaluate cellular uptake, targeted drug delivery, and controllable release.

Materials and Methods

Material

Curcumin and β-CD were purchased from GuangLin Biological Pharmaceutical Co. Ltd. (Hangzhou, China) and Boao Biotechnology Co. Ltd. (Shanghai, China), respectively. Stannous 2-ethylhexanoate [Sn(Oct)2] was purchased from Sigma-Aldrich (St. Louis, MO). Dialysis bags [molecular weight cut-off (MWCO)= 14,000 Da) were purchased from Gene Star Co. (Shanghai, China). Other chemical reagents, including FA, 3-(4,5-dimethylthiazol-2-yl)-2,5-diphenyltetrazolium bromide (MTT), fetal bovine serum (FBS), and N, N-carbonyldiimidazole (CDI) were obtained from Aladdin Chemicals (Shanghai, China). Dulbecco's modified Eagle's medium (DMEM) was purchasedfromThermo FisherScientificSuzhou Co., Ltd (Suzhou, China). HeLa cells and L929 mouse embryonic fibroblasts were obtained from the Cell Resource Center, Shanghai Institute of Life Sciences, Chinese Academy of Sciences (Shanghai, China) and the Cell Bank of the

Chinese Academy of Sciences (Beijing, China), respectively.

Synthesis of β-CD-Polycaprolactone Copolymers (β-CD-CL)

β-CD-CL copolymers were synthesized by ring-opening polymerization of caprolactone monomers in the presence of β-CD taking stannous octoate (0.1% w/w) as a catalyst with a β-CD: ε-CL ratio of 1:210 (w/w). The reaction was performed for 36h at 120°C under dry nitrogen. The obtained copolymers were dissolved in dichloromethane (15 mL) and then purified by precipitation in ether. The purification process was repeated three times, and the product was obtained and vacuum drying at 40°C. The structure of the β-CD-CL copolymers was confirmed by Fourier transform infrared (FT-IR) spectroscopy (Nicolet 6700; Thermo Fisher Scientific, Waltham. MA) and ^{1}H-nuclear magnetic resonance (^{1}H-NMR) spectroscopy (AC-III, 500 MHz; Bruker Daltonics, Billerica, MA).

Preparation of Folate-Conjugated β-CD-CL Block Copolymers (β-CD-CL-FA)

β-CD-CL-FA block copolymers were synthesized according to a previous report.[30] Briefly, β-CD-CL copolymers (0.05 mmol) were activated by adding CDI (0.35 mmol) and triethylamine (TEA;0.35 mmol) in DMSO (10 mL) at 25°C in nitrogen atmosphere for 6 h. Then, FA solution was prepared by dissolving FA (0.35 mmol) in DMSO (1 mL) and added dropwise to the activated β-CD-CL copolymer solution. Afterwards, the solution was stirred in nitrogen atmosphere darkly for 24 h at 25°C. The obtained solution was dialyzed in a dialysis bag (MWCO =14,000 Da) for 72 h to remove the organic solvent, unreacted monomers and oligomers. Finally, β-CD-CL-FAcopolymers were lyophilized for further use. The structure of the β-CD-CL-FA copolymers was confirmed by FT-IR spectroscopy and ^{1}H-NMR spectroscopy.

Preparation and Characterization of Curcumin Loaded β-CD-CL Nanoparticles (Cur-NPs) and β-CD-CL-FA Nanoparticles (FA-Cur-NPs)

FA-Cur-NPs and Cur-NPs were fabricated as previously described.[31,32] The optimal conditions were as follows: a total of 7 mg β-CD-CL-FA or β-CD-CL and 1.4 mg of curcumin were dissolved in 1mL acetone and added dropwise to 10mL purified water. The mixture was stirred at 600 rpm for 4 h at 37°C, after which the obtained nano-preparations (FA-Cur-NP and Cur-NP suspensions) were centrifuged at 4000 g for 30 min to remove the unencapsulated curcumin. Blank β-CD-CL nanoparticles (blank NPs) and blank β-CD-CL-FA nanoparticles (FA-NPs) were prepared in the same manner as Cur-NPs and FA-Cur-NPs (without Cur in the acetone), respectively. Particle size, polydispersion index (PDI), and zeta potential of FA-Cur-NPs and Cur-NPs were measured by a laser particle analyzer (Zetasizer NanoZS90; Malvern Panalytical, Malvern, UK). Additionally, the amount of drug present in the FA-Cur-NPs was determined by ultraviolet spectrophotometry (UV-2102; Shanghai Instrument Ltd., Shanghai, China) at a detection wavelength of 420 nm. The drug loading (DL) and entrapment efficiency (EE) of FA-Cur-NPs and Cur-NPs were calculated against the standard curve using the following equations:

$$\mathrm{EE\%} = \frac{\text{weight of drug in nanoparticles}}{\text{weight of feed drug}} \times 100\% \quad (1)$$

$$\mathrm{DL\%} = \frac{\text{weight of drug in nanoparticles}}{\text{weight of nanoparticles}} \times 100\% \quad (2)$$

Transmission Electron Microscopy (TEM)

TEM was used to analyze the microstructure of FA-Cur-NPs and Cur-NPs at a magnification of 20,000×. A droplet of the nano-preparations was placed on a film-coated copper grid, then 1% (w/v) phosphotungstic acid was placed onto the surface of the sample-loaded grid. Finally, the sample was air-dried and imaged using TEM (JEM-1010; Jeol Ltd., Tokyo, Japan).

X-Ray Diffraction (XRD)

To verify the distribution of curcumin in the nanoparticles, the surface properties of curcumin, FA-NPs, and FA-Cur-NPs were measured by XRD analysis at an output voltage of 40 kV, output current of 40 mA, and a wavelength of 0.1546 nm. The samples were freeze-dried before measurement.

Stability Study

FA-Cur-NPs (1 mL) and DMEM (8 mL, containing 10% FBS complete medium) were co-incubated at 37°C for 72 h. At the indicated time points (1, 2, 4, 8, 24, 48, and 72 h), 1 mL of the mixture solution was removed, and the sample was treated with excess acetonitrile to remove the serum

protein. The supernatant was collected, and the variation in particle diameter and PDI were monitored using a granulometer (Zetasizer NanoS90; Malvern Panalytical). All experiments were carried out in triplicate.

In vitro Drug Release

Release behavior of FA-Cur-NPs in vitro was investigated using dialysis. Briefly, FA-Cur-NPs with a curcumin content of 150 μg/mL was prepared and placed in a dialysis bag (MWCO =14,000 Da). Subsequently, the dialysis bags were transferred into 50 mL of pH 7.4, 6.4, and 5.0 PBS and shaken at 700 rpm and 37±0.5°C for 120 h. At the indicated time points (1, 2, 4, 6, 12, 24, 36, 48, 60, 72, 96, and 120 h), 4 mL of release medium was removed for analysis and replaced by an equivalent volume of fresh dissolution medium.

In vitro Cytotoxicity

L929 cells and HeLa cells (human cervical cancer cell line) were cultured in 96-well plates at a density of 1.0×10^5 per well in 100 μL growth medium supplemented with 10% (v/v) FBS and 1% (v/v) penicillin/streptomycin at 37°C and 5% CO_2 for 24 h before the addition of various nanoparticles. HeLa cells were cultured in DMEM while L929 cells were cultured in RPMI 1640 medium. L929 cells were co-cultured with various doses of sterilized blank NPs, FA-NPs, free FA+FA-NPs (0.5 mg/mL free FA was added to pre-incubate for 30 min before FA-NPs were added), or medium (negative control) for 24 h to assess the biosafety. HeLa cells were co-cultured with various doses of sterilized curcumin-loaded nanoparticles (Cur-NPs, FA-Cur-NPs, and free FA + FA-Cur-NPs) or medium (negative control) for 24 h to evaluate the antitumor effect in vitro. Thereafter, cell viability was quantified using the MTT assay.[32] All samples were prepared in triplicate. Furthermore, the IC50 value of each carrier was calculated.

Cellular Uptake

HeLa cells were seeded in a 6-well plate at a density of 2×10^5 cells per well in 2 mL growth medium and incubated for 24 h at 37°C and 5% CO_2. The medium was then replaced with 2 mL of fresh DMEM medium containing Cur-NPs, FA-Cur-NPs, or FA+FA-Cur-NPs with a curcumin content of 30 μg/mL and co-cultured for 3 h. Fluorescence microscopy (1×73P1F; Olympus, Tokyo, Japan) was used to evaluate cellular uptake at a magnification of 200×.

Flow Cytometry

HeLa cells were seeded in a 6-well plate at a density of 5×10^5 cells per well and incubated for 24 h. Subsequently, the medium was replaced by fresh medium containing Cur-NPs, FA-Cur-NPs, or FA+FA-Cur-NPs with a curcumin content of 30 μg/mL. HeLa cells without any treatment were used as the control group. The cells were incubated for 3 h and rinsed three times with PBS. Then, cells were harvested by trypsin and centrifuged at 100 g for 5 min. Finally, cells were resuspended in PBS and analyzed by flow cytometry (CytoFLEX; Beckman Coulter, Brea, CA).

Animal Model

Female BALB/c nude mice (weighing 15–17g, 4 weeks old) were obtained from Zhejiang Academy of Medical Sciences (Hangzhou, China). All mouse experiments were approved by the Ethics Committee of Zhejiang University of Technology (No. 39/2018). All experimental procedures were conducted in accordance with the Institutional Animal Care and Use Committee (IACUC) and use of laboratory animals at Zhejiang University of Technology and the National Institutes of Health Guide for Care and Use of Laboratory Animals (publication no. 85–23, revised 1996). The nude mice were acclimatized for 4 days after arrival. HeLa cells (1×10^7, 0.2 mL) was subcutaneously inoculated into the left foreleg of mice to establish cervical carcinoma xenografts. When the tumors reached an average volume of ~100 mm^3, we evaluated biodistribution and antitumor activity in vivo.

Biodistribution

Cur-DMSO [0.2 mL of 6.25 mg/kg; DMSO: H_2O 1:1000(v/v)] aqueous solution (control group), Cur-NPs, or FA-Cur-NPs were injected into tumor-bearing mice via the tail vein. Thereafter, mice were anesthetized at 3 and 7 h, and images of curcumin biodistribution in vivo were obtained with a small animal imager (IVIS Lumina XRMS III; PerkinElmer, Waltham, MA) at excitation and emission wavelengths of 488 nm and 520 nm, respectively. After 8 h, the mice were sacrificed, and the tumors, heart, liver, spleen, lungs, and kidneys were collected. The fluorescence intensity of these organs was also examined by the small animal imager.

In vivo Antitumor Activity and Histological Analysis

The tumor-bearing mice were randomized into four groups (n=5/group); a single administration of saline (negative

control) or a 6.25 mg/kg of Cur-DMSO, Cur-NPs, or FA-Cur-NPs was injected via tail vein (0.2 mL) every three days. Weights and tumor volumes were recorded. After thirty days treatment, the mice were sacrificed, after which the main organs (heart, liver, spleen, lungs, kidneys, and tumors) were weighed and fixed in 4% paraformaldehyde. Histological sections were then prepared stained with hematoxylin and eosin (H&E).

Statistical Analysis

Statistical analysis was carried out by SPSS 19.0 (SPSS, IBM, Armonk, NY, USA) using a two-tailed *t*-test and analysis of variance (ANOVA). Data are presented as the mean ± standard deviation (SD). P-values < 0.05 were considered statistically significant. All experiments were conducted at least three times.

Results and Discussion

Synthesis and Characterization of β-CD-CL-FA Copolymers

FT-IR is one of the main methods used to determine the functional groups of compounds. The FT-IR spectra of β-CD, β-CD-CL, and β-CD-CL-FA are shown in Figure 1A. For β-CD, the peak at 3394.1 cm^{-1} corresponds to hydroxyl (-OH) bond stretching, while the peaks at 2935.3 and 1417.4 cm^{-1} are attributed to the asymmetric stretching vibration and in-plane bending vibration of methylene (-CH_2-), respectively. Compared with those of β-CD and β-CD-CL, the newly emerged characteristic peaks of β-CD-CL at 2867.5 and 1726.7 cm^{-1} reflect the methylene (-CH_2-) and ester group (C=O) corresponding to the stretching vibration of the PCL fragments. Additionally, the strength of the -OH stretching vibration peak (3439.9 cm^{-1}) was greatly weakened, indicating that the primary hydroxyl group on β-CD was displaced. Based on these results, the covalent grafting between β-CD and ε-CL were successfully reacted, and fabrication of β-CD-CL was achieved. A further comparative analysis between β-CD-CL-FA and β-CD-CL demonstrated that the characteristic peaks of FA appeared at 1607.2 and 1512.9 cm^{-1}, which were attributed to the benzene ring skeleton (C=C), indicating that β-CD-CL-FA was successfully synthesized.

The ^{1}H-NMR spectra and peak assignments of β-CD-CL-FA are shown in Figure 1B. The chemical shifts of the methylene group (-CH_2-), hydroxyl (-OH), and N-H bonds (-NH-) in FA was observed at 4.48 ppm (4), 11.44 ppm (2), and 6.95 ppm (5), respectively. Peaks at 8.65 ppm (3), 7.64 ppm (6), 6.64ppm (7), and 4.32 ppm (9) correspond to the C-H bonds of FA. For the β-CD-CL unit, the methylene group (-CH_2-) peaks were at 3.99 ppm (a), 1.30 ppm (b), 2.28 ppm (c), 1.54 ppm (d), while those at 5.70 ppm (f), 4.48 ppm (g) and 4.83 ppm (h) correspond to the C-H bonds. Moreover, the chemical shift of the (-CH_2-) group in FA and the (C-H) group in β-CD-CL overlapped at 4.48 ppm.

Additionally, the ratio of the integral of the hydrogen between β-CD (e-h) and ε-CL (a-d) was 1:7, demonstrating that the seven chains of β-CD were modified by ε-CL. Similarly, for β-CD-CL-FA, the value of FA: β-CD-CL was 7:1, indicating that FA was attached to each branch

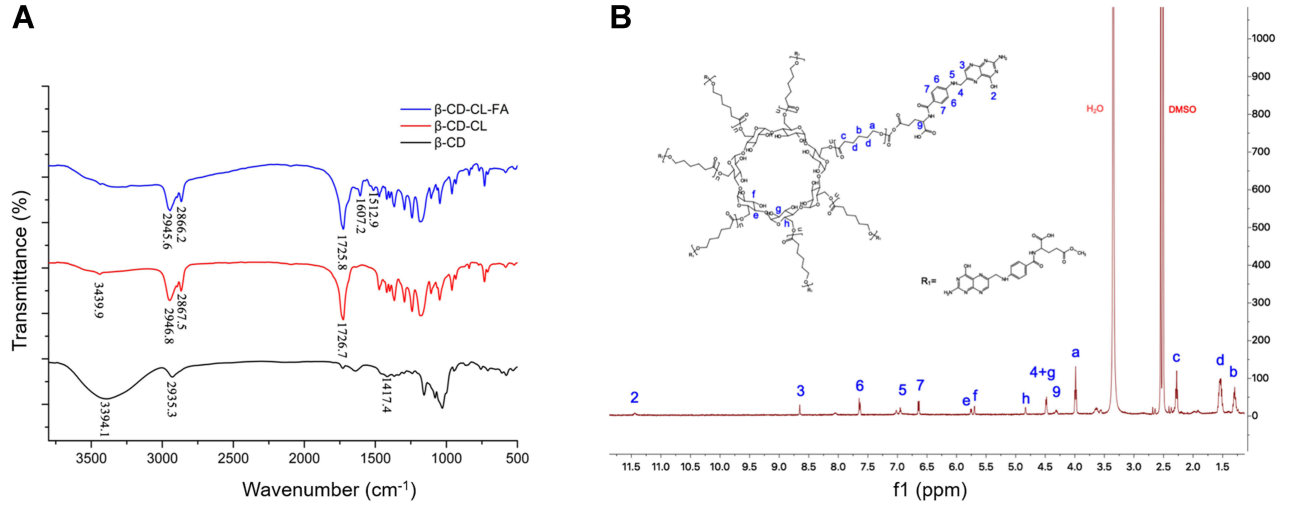

Figure 1 Characterization of copolymers. (**A**) FT-IR spectra of β-CD, β-CD-CL, and β-CD-CL-FA, (**B**) ^{1}H-NMR spectra of β-CD-CL-FA.
Abbreviations: FT-IR, Fourier transform infrared; ^{1}H-NMR, ^{1}H-nuclear magnetic resonance; β-CD, β-cyclodextrin; β-CD-CL, β-CD-polycaprolactone copolymers; β-CD-CL-FA, folate-conjugated β-CD-CL block copolymers.

of β-CD-CL. Altogether, the results indicate that the seven chains of β-CD are connected to ε-CL, and each branch of β-CD-CL is also modified by FA. Thus, β-CD-CL and β-CD-CL-FA were successfully synthesized.

Characterization of Curcumin-Loaded Nanoparticles

The prepared nanoparticles were characterized by TEM and laser particle analyzer (Table 1 and Figure 2A–C). Both FA-Cur-NPs and Cur-NPs exhibited a near-spherical nano-sized shape that was approximately 150 nm in size with a narrow distribution (PDI<0.1) and negative zeta potential. The DL of FA-Cur-NPs was slightly higher than that of Cur-NPs, while their EE was similar. The DL values were greater than 15%, indicating a high drug-loaded delivery system. Moreover, XRD analysis showed almost overlapping FA-Cur-NPs and Cur-NPs lines, while the characteristic peaks of native curcumin disappeared in Cur-P-NPs. XRD results indicated that curcumin was trapped in the FA-Cur-NPs (Figure 2D).

Stability of FA-Cur-NPs

The stable structure of nanocarriers in the physiological environment is a critical element for obtaining excellent drug delivery systems. To evaluate the stability of FA-Cur-NPs in blood, FA-Cur-NPs were mixed with DMEM supplemented with 10% FBS (simulated blood environment) and incubated at 37°C for 72 h. The variation in particle size and PDI was monitored, and the results are shown in Figure 2F. During the first 4 h, the particle size and PDI of FA-Cur-NPs increased slightly, then remained stable until 72 h, indicating that the FA-Cur-NPs have excellent stability.[33]

In vitro Drug Release

For FA-Cur-NPs, we assessed in vitro drug release at 37°C at pH 7.4, 6.4, and 5.0 to mimic the pH conditions of systemic circulation, the slightly acidic tumor environment, and intracellular lysosomes, respectively. As shown in Figure 2E, all release curves showed a fast release rate in the first 6 h followed by a slow-release phase. These results are consistent with the regulation of drug release by free diffusion. Curcumin on the surface or in superficial layers of the FA-Cur-NPs was easily diffused into the releasing medium, in contrast to the encapsulated curcumin; this led to a fast release rate in the first phase driven by osmotic diffusion and material degradation, followed by a slow-release phase mainly driven by the degradation of nanoparticles. Moreover, the slowest released pattern was measured in pH 7.4 buffer, where only 20.89% of curcumin was released after 120 h of incubation. On the other hand, at pH 6.4 and 5.0, the release curves were similar in the fast release phase; thereafter, the cumulative release rate of curcumin reached 62.31% and 72.18% at 120 h, respectively. Due to the accelerated degradation of ester bonds in weakly acidic environments,[34] the releasing medium could more easily diffuse into the inner layers of the nanoparticles; thus, FA-Cur-NPs displayed a faster release rate at pH 6.4 and 5.0 than at pH 7.4. Additionally, due to the stronger degradation efficiency of the ester bonds, FA-Cur-NPs showed a faster release rate in the second phase at pH 5.0 than at pH 6.4, indicating that curcumin is released from FA-Cur-NPs faster and at a greater extent after entering tumor cells. These results demonstrate that the FA-Cur-NP delivery system can overcome the problem of fast drug release in a β-CD-based nano delivery system and achieve slow drug release. Moreover, as the release rate of curcumin from FA-Cur-NPs was 3-folds faster at pH 6.4 (tumor microenvironment) than at pH 7.4 (systemic circulation), more curcumin can be enriched around the tumor than around normal cells, indicating potentially enhanced antitumor therapeutic effects and reduced toxicity and adverse side effects during treatment.

Table 1 Characterization of Curcumin-Loaded Nanoparticles

Characteristics	Cur-NPs	FA-Cur-NPs
Mean diameter (nm)	127.4±1.9	151.8±1.3
Polydispersity index	0.095±0.026	0.073±0.024
Zeta potential (mV)	−7.06±0.46	−15.81±1.05
Encapsulation efficiency (%)	96.24±1.89	95.64±0.92
Drug loading (%)	17.51±1.93	20.27±1.36

In vitro Cytotoxicity

To assess biosafety, we performed MTT assays with the fibroblast L929 cells as model cells after 24 h of incubation with the nanoparticles. As shown in Figure 3A, cell viability in the presence of blank NPs, FA-NPs, and free FA+FA-NPs slightly decreased as the concentration increased from 0.25 to 1.20mg/mL. However, the cell viability of all samples was above 85% when the carrier concentration reached 1.2 mg/mL, indicating good biocompatibility of all groups.

In vitro Anticancer Activity

Folate receptor (FR)-positive HeLa cells were chosen, and the cell viability was assayed by MTT to evaluate the anticancer activity of different curcumin-loaded nanoparticles at curcumin concentrations of 2.5–40 μg/mL in vitro. As shown in Figure 3B, all curcumin-loaded carriers exhibited anticancer

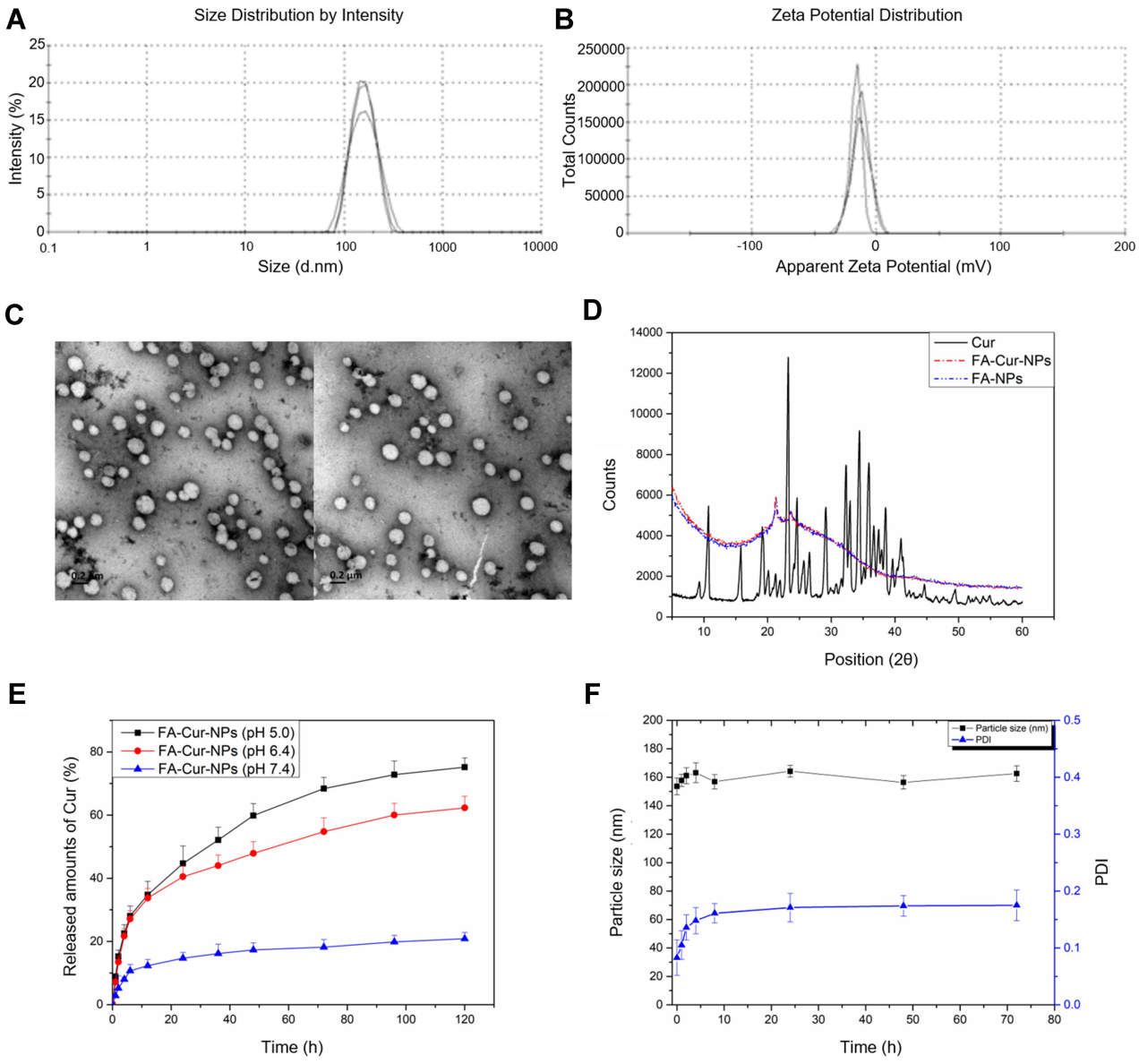

Figure 2 Characterization of nanoparticles. (**A**) Particle size and (**B**) zeta potential of FA-Cur-NPs, (**C**) TEM image of FA-Cur-NPs (left) and Cur-NPs (right), (**D**) X-ray diffraction curve of curcumin (Cur), FA-NPs, and FA-Cur-NPs, (**E**) In vitro release profiles of curcumin from FA-Cur-NPs at different pH values, (**F**) In vitro stability of FA-Cur-NPs in DMEM supplemented with 10% FBS at 37°C for 72h (n=3).

Abbreviations: TEM, transmission electron microscopy; FA-Cur-NPs, curcumin-loadedβ-CD-CL-FA nanoparticles; Cur-NPs, curcumin-loadedβ-CD-CL nanoparticles; FA-NPs, blank β-CD-CL-FA nanoparticles; DMEM, Dulbecco's modified Eagle's medium;FBS, fetal bovine serum.

activity in a curcumin dose-dependent manner. Additionally, the IC50 values of Cur-NPs, FA-Cur-NPs, and free FA+FA-Cur-NPs for HeLa cells were 27.34, 13.88, and 20.53 μg/mL, respectively, showing decreasing anticancer effects in the order FA-Cur-NPs > free FA+FA-Cur-NPs > Cur-NPs. Moreover, free FA was pre-incubated with HeLa cells to analyze FR-mediated endocytosis of FA-Cur-NPs. Comparing with free FA+FA-Cur-NPs, FA-Cur-NPs displayed stronger anticancer activity, indicating the superior cytotoxic activity of FA-Cur-NPs through FR-mediated endocytosis pathways. Moreover, the growth inhibition effect of FA-Cur-NPs on HeLa cells was significantly stronger than that of Cur-NPs, which can be explained by the same principle. We performed further cellular uptake studies to confirm these findings.

Cellular Uptake

Cellular uptake efficiency of curcumin-loaded nanoparticles was investigated by fluorescence microscopy (Figure 4A) and quantitatively by flow cytometry

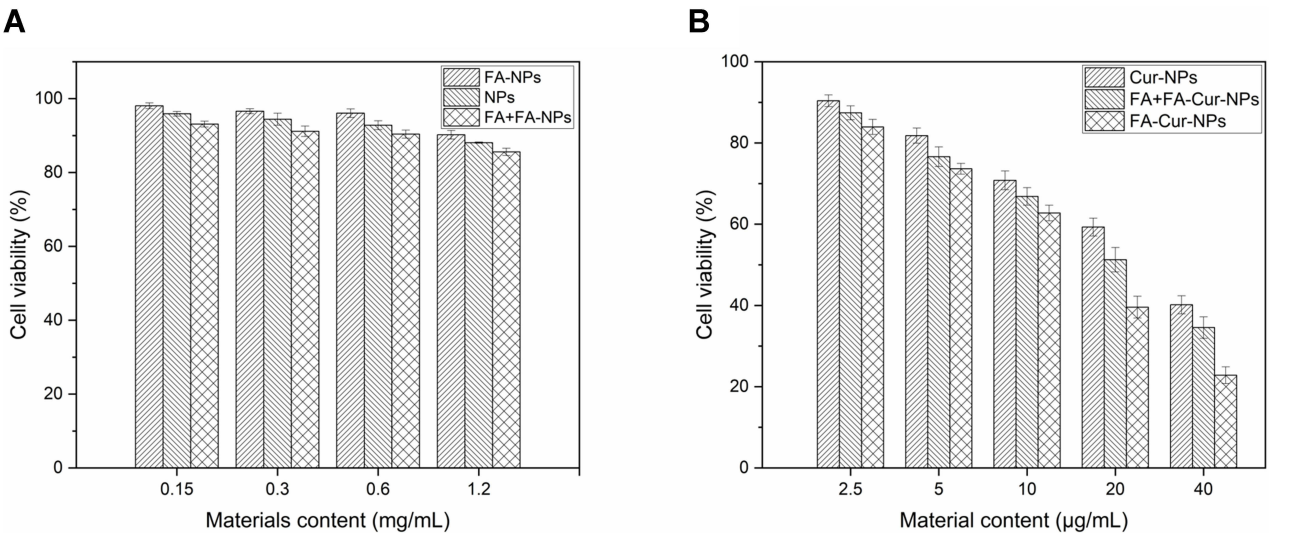

Figure 3 In vitro cytotoxicity and anticancer activity. (**A**) Cytotoxicity of blank NPs, FA-NPs, and free FA+FA-NPs after incubation with L929 cells, (**B**) Cell viability of HeLa cells in the presence of Cur-NPs, free FA+FA-Cur-NPs, and FA-Cur-NPs.
Abbreviations: blank NPs, blank β-CD-CL nanoparticles; FA-NPs, blank β-CD-CL-FA nanoparticles; Cur-NPs, curcumin-loadedβ-CD-CLnanoparticles; FA-Cur-NPs, curcumin-loadedβ-CD-CL-FA nanoparticles.

(Figure 4B). Compared with control, HeLa cells treated with curcumin-loaded nanoparticles exhibited higher fluorescence intensities, indicating that the nanoparticles were successfully internalized by HeLa cells. Internalization occurred at different extents, as the fluorescence intensity decreased in the order FA-Cur-NPs > free FA+FA-Cur-NPs > Cur-NPs. The results obtained by fluorescence microscopy was consistent with that of flow cytometry. The lower fluorescence intensity of free FA+FA-Cur-NPs compared with the FA-Cur-NPs indicates that the internalization of FA-Cur-NPs was followed by FR-mediated endocytosis. Moreover, the mean fluorescence intensity values of free FA+FA-Cur-NPs and FA-Cur-NPs were 1.8- and1.6-folds higher than that of Cur-NPs, respectively, suggesting that FR-mediated endocytosis contributes to the enhanced drug uptake.[35] These findings are consistent with those of the in vitro anticancer activity assay, supporting the superior cytotoxic activity of FA-Cur-NPs through FR-mediated endocytosis pathways. Thus, we can speculate that polymeric nanoparticles based on FA as a targeting molecule have great potential as vehicles for anticancer drug delivery.

In vivo and ex vivo Imaging

The tumor-targeting ability of the developed FA-Cur-NPs was assessed in a HeLa xenograft mouse model by in vivo and ex vivo near-infrared fluorescence (NIRF) imaging (Figure 5A). After injecting Cur-DMSO, a small amount of curcumin was found accumulated in the tumor site at 3h. Thereafter, most of the curcumin was distributed throughout the body at 7 h, with no sign of specific tumor targeting. In contrast, the fluorescence intensity in the tumor sites of both nanoparticle groups was higher than that of the Cur-DMSO group. This may have resulted from the enhanced permeability and retention (EPR) effect (passive targeting) and the interaction between FA and FR (active targeting). The biodistribution of intravenously injected nanoparticles was observed by ex vivo NIRF imaging 7h after injection (Figure 5B). The fluorescence intensity of the Cur-DMSO group in the liver and kidney was significantly higher than that of the other two nanoparticle groups, while the highest fluorescence intensity was observed in tumors in the FA-Cur-NP group. These results support the successful tethering of FA onto the nanoparticles and in vivo tumor targetability after intravenous injection. FR-mediated endocytosis pathways are considered responsible for the more efficient accumulation of FA-Cur-NPs in the tumor sites. These results are also consistent with those of the cellular uptake study.

In vivo Suppression of Tumor Growth

The in vivo antitumor ability of FA-Cur-NPs using the HeLa-xenograft mouse model was further assessed. Tumor-bearing mice were treated with saline (control group), Cur-DMSO, Cur-NPs, or FA-Cur-NPs. Tumor growth was significantly inhibited in the experimental

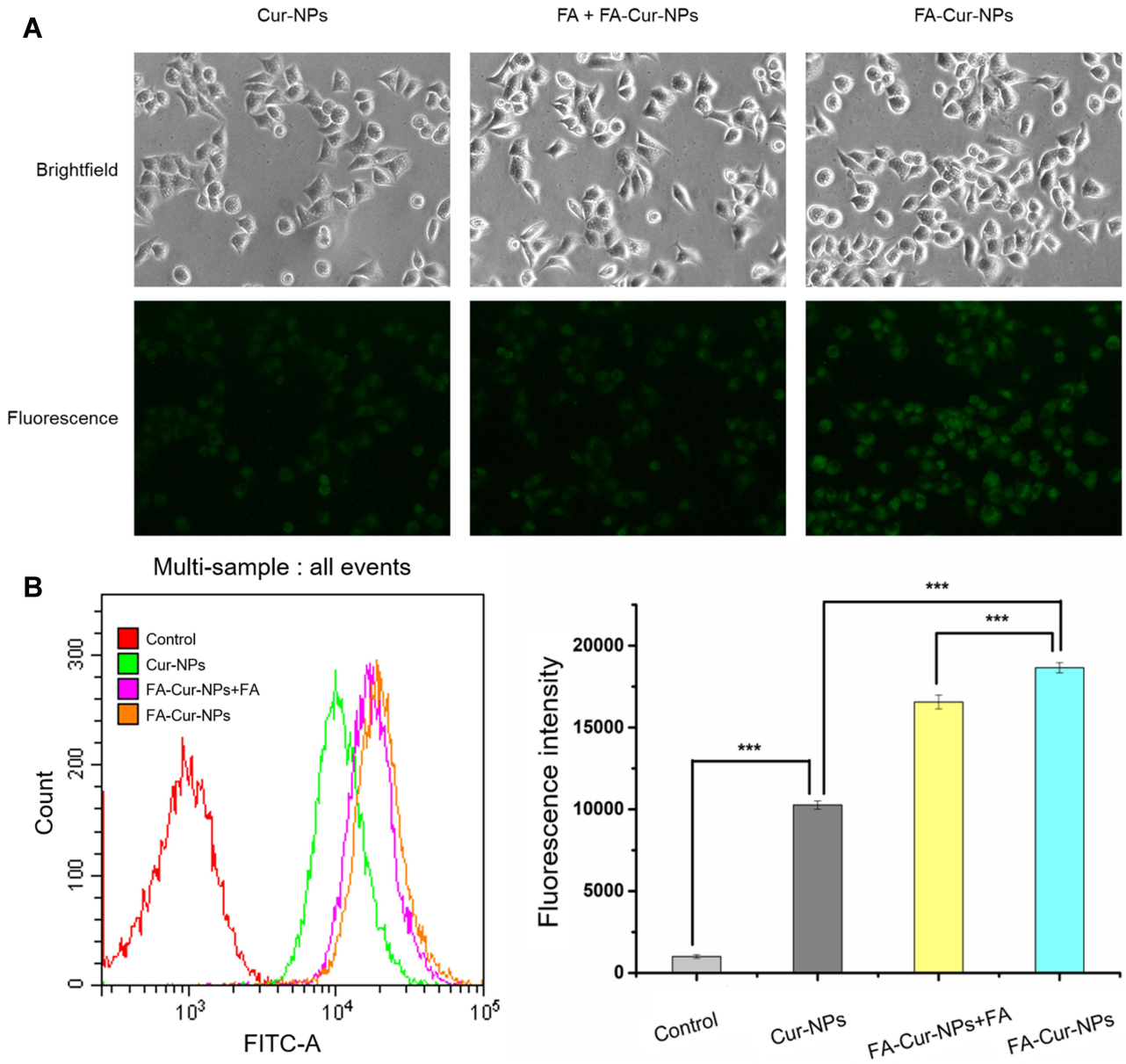

Figure 4 Cellular uptake in HeLa cells. (**A**) Cellular uptake of Cur-NPs, free FA+FA-Cur-NPs, and FA-Cur-NPs, (**B**) Flow cytometry profiles of HeLa cells incubated with Cur-NPs, free FA+FA-Cur-NPs, and FA-Cur-NPs for 3 h. Fluorescence intensity values are shown (n=4). ***P < 0.001.
Abbreviations: Cur-NPs, curcumin-loadedβ-CD-CLnanoparticles; FA-Cur-NPs, curcumin-loadedβ-CD-CL-FA nanoparticles.

groups compared to the control group. Tumor growth profiles revealed that tumor volumes increased nearly 30-, 22-, 16-, and 5-fold after 30 days when treated with saline, Cur-DMSO, Cur-NPs, and FA-Cur-NPs, respectively (Figure 5C). Tumor growth inhibition is attributed to passive targeting achieved by the EPR effect, as nanoparticles with a size < 300 nm can pass through the leaky vasculature to access tumors. In addition, the tumor inhibitory effect was significantly higher in the FA-Cur-NP group than in the others. This enhanced antitumor activity can be attributed to the EPR effect and active targeting of FA. Meanwhile, the body weight profiles showed that the body weights of mice treated with Cur-DMSO, Cur-NPs, and FA-Cur-NPs did not change significantly, whereas mice in the control group lost more than 15% body weight after 30 days, indicating reduced side effects associated with the nanoparticles (Figure 5D). Furthermore, tumor volume and body weight were negatively correlated, where rapid growth of the tumor corresponded to a decrease in body weight.

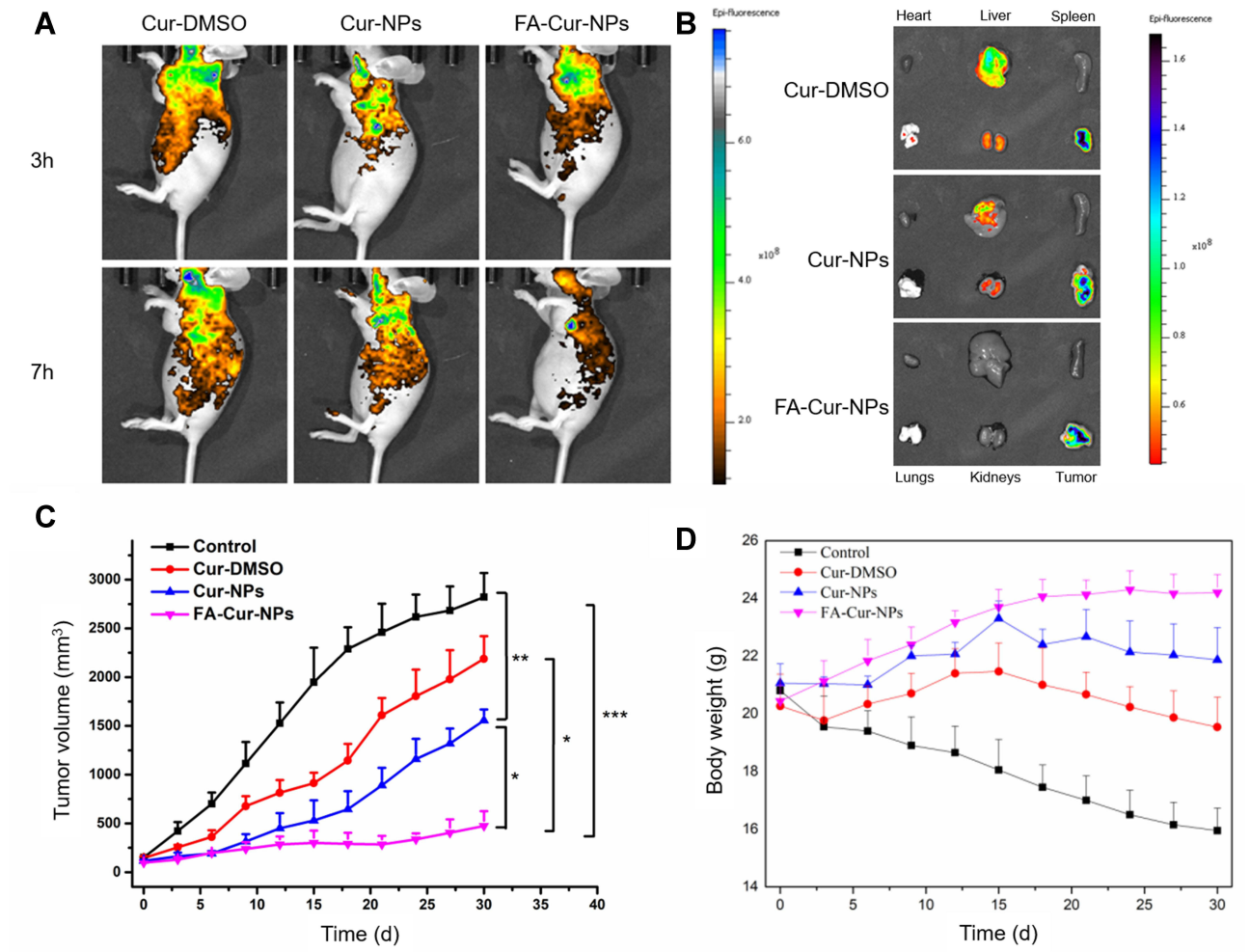

Figure 5 Biodistribution and antitumor efficacy (**A**) Whole-body NIRF imaging of a HeLa xenograft mouse model, (**B**) Ex vivo NIRF image of dissected organs and tissues (liver, spleen, kidney, heart, lung, and tumor), (**C**) Tumor volume and (**D**) body weight after intravenous administration of the indicated preparations.*P < 0.05, **P < 0.01, ***P < 0.001.
Abbreviation: NIRF, near-infrared fluorescence.

H&E staining of the major organs showed no discernible injuries after treatment with FA-Cur-NPs (Figure 6). There was a marked infiltration of lymphocytes in the liver and kidney in Cur-DMSO and Cur-NP groups. H&E staining also confirmed that FA-Cur-NPs show the most enhanced therapeutic efficacy, as evidenced by the large area of tissue necrosis in the tumor. Considering that the only difference between Cur-NPs and FA-Cur-NPs is the folate linkage to β-CD-CL copolymers, we can attribute the enhanced therapeutic efficiency to FA-induced accumulation and cellular internalization in tumor tissues. These results also demonstrate the high biosafety of FA-Cur-NPs.

Conclusion

Here, a novel FR-targeted drug delivery system using curcumin for cervical cancer treatment was fabricated. To this end, a β-CD-CL copolymer was synthesized and conjugated with folate, which was then formulated as nanoparticles by emulsion-solvent evaporation. The carrier showed good biocompatibility, targeting ability, and high drug loading capacity with a curcumin loading rate of 20.27±0.92% and EE of 95.64 ±0.92%. The in vitro release rate of curcumin from FA-Cur-NPs under tumor microenvironment conditions (pH 6.4) was three times faster than that under systemic circulation conditions (pH 7.4), demonstrating that the delivery system is suitable for rapid drug release in the tumor microenvironment. Moreover, FA-Cur-NPs showed significantly improved therapeutic efficacy in vivo. FA was thus successfully utilized as both a tumor-targeting moiety and ligand to enhance cellular internalization. Therefore, this nanocarrier can provide insights into improving the design of drug delivery systems and represents a potential strategy for cancer therapy.

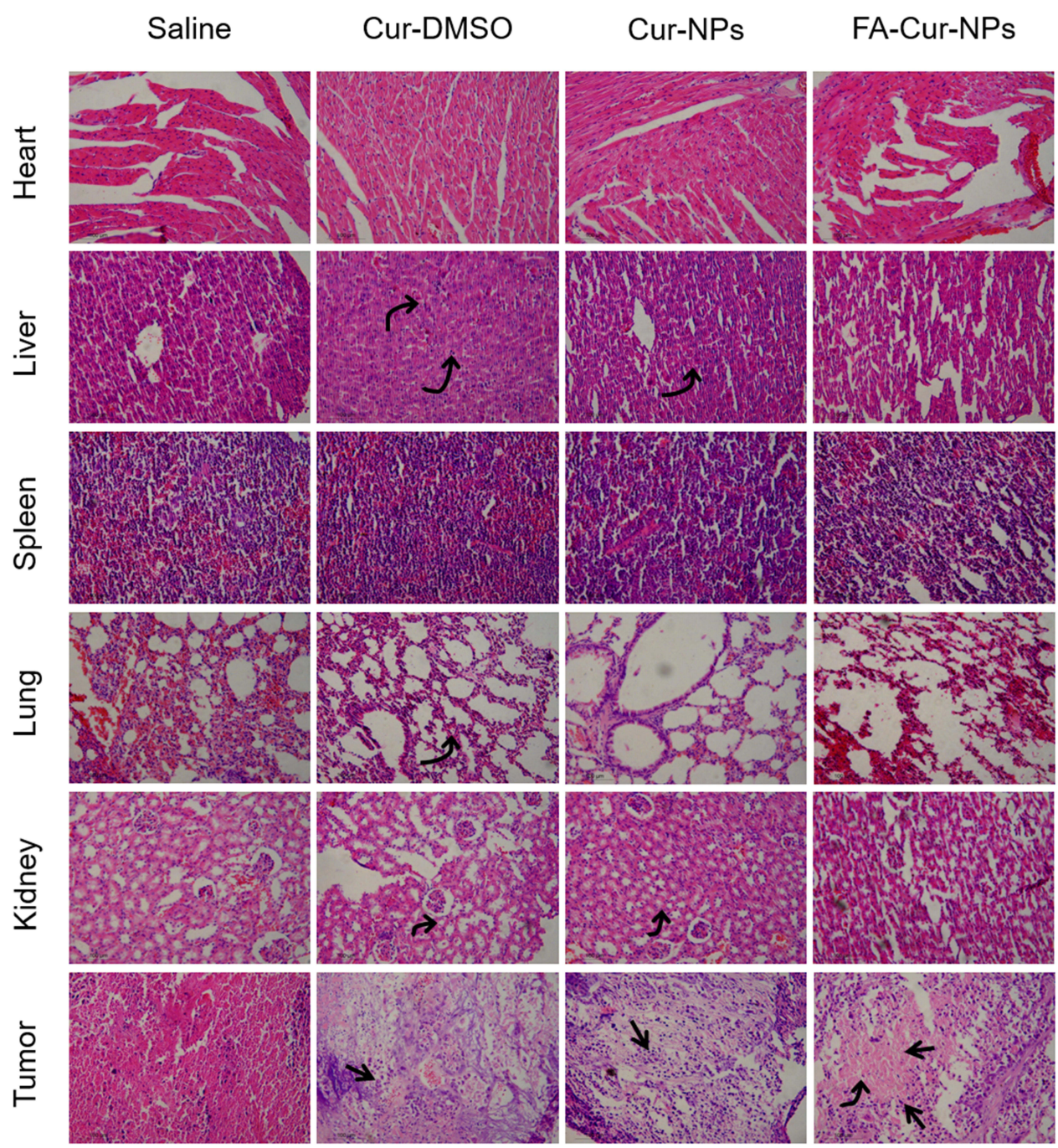

Figure 6 H&E-stained sections of organs resected from mice sacrificed 30 days after treatment. Straight arrows indicate tissue necrosis, and curved arrows indicate lymphoid infiltration.
Abbreviation: H&E, hematoxylin-eosin.

Acknowledgments

This research was financially supported by the National Natural Science Foundation of China (No. 22078297), Zhejiang Provincial Natural Science Foundation of China (LY19B060012), Science and Technology Plan Project of Taizhou (1901ky49), Special Research Fund of Hospital Pharmacy of Zhejiang Pharmaceutical Association (2019ZYY44, 2017ZYY28).

Disclosure

The authors report no conflicts of interest in this work.

References

1. Sung H, Ferlay J, Siegel RL, et al. Global cancer statistics 2020: GLOBOCAN estimates of incidence and mortality worldwide for 36 cancers in 185 countries. *CA Cancer J Clin*. 2021;71:209–249. doi:10.3322/caac.21660
2. Kamran SC, D'Amico AV. Radiation therapy for prostate cancer. *Hematol Oncol Clin North Am*. 2020;34(1):45–69. doi:10.1016/j.hoc.2019.08.017
3. Kumar L, Harish P, Malik PS, Khurana S. Chemotherapy and targeted therapy in the management of cervical cancer. *Curr Probl Cancer*. 2018;42(2):120–128. doi:10.1016/j.currproblcancer.2018.01.016
4. Samadani AA, Keymoradzdeh A, Shams S, et al. CAR T-cells profiling in carcinogenesis and tumorigenesis: an overview of CAR T-cells cancer therapy. *Int Immunopharmacol*. 2021;90:107201. doi:10.1016/j.intimp.2020.107201
5. Liu J, Zheng Y, Xu N. Low dose of apatinib in treating chemotherapy and EGFR-TKI refractory non-small cell lung cancer: a case report. *Medicine (Baltimore)*. 2019;98(5):e14328. doi:10.1097/MD.0000000000014328
6. Cheng YJ, Hu JJ, Qin SY, Zhang AQ, Zhang XZ. Recent advances in functional mesoporous silica-based nanoplatforms for combinational photo-chemotherapy of cancer. *Biomaterials*. 2020;232:119738. doi:10.1016/j.biomaterials.2019.119738
7. Muhamad N, Plengsuriyakarn T, Na-Bangchang K. Application of active targeting nanoparticle delivery system for chemotherapeutic drugs and traditional/herbal medicines in cancer therapy: a systematic review. *Int J Nanomedicine*. 2018;13:3921–3935. doi:10.2147/IJN.S165210
8. Hussain Z, Thu HE, Amjad MW, et al. Exploring recent developments to improve antioxidant, anti-inflammatory and antimicrobial efficacy of curcumin: a review of new trends and future perspectives. *Mater Sci Eng C Mater Biol Appl*. 2017;77:1316–1326. doi:10.1016/j.msec.2017.03.226
9. Lal B, Kapoor AK, Agrawal PK, Asthana OP, Srimal RC. Role of curcumin in idiopathic inflammatory orbital pseudotumours. *Phytother Res*. 2000;14(6):443–447. doi:10.1002/1099-1573-(200009)14:6<443::aid-ptr619>3.0.co;2-v
10. Zhao X, Chen Q, Li Y, et al. Doxorubicin and curcumin co-delivery by lipid nanoparticles for enhanced treatment of diethylnitrosamine-induced hepatocellular carcinoma in mice. *Eur J Pharm Biopharm*. 2015;93:27–36. doi:10.1016/j.ejpb.2015.03.003
11. Dasi F, Martinez-Rodes P, March JA, et al. Real-time quantification of human telomerase reverse transcriptase mRNA in the plasma of patients with prostate cancer. *Ann N Y Acad Sci*. 2006;1075:204–210. doi:10.1196/annals.1368.028
12. Kumar P, Barua CC, Sulakhiya K, Sharma RK. Curcumin ameliorates cisplatin-induced nephrotoxicity and potentiates its anticancer activity in SD rats: potential role of curcumin in breast cancer chemotherapy. *Front Pharmacol*. 2017;8:132. doi:10.3389/fphar.2017.00132
13. Rezaee R, Momtazi AA, Monemi A, Sahebkar A. Curcumin: a potentially powerful tool to reverse cisplatin-induced toxicity. *Pharmacol Res*. 2017;117:218–227. doi:10.1016/j.phrs.2016.12.037
14. Yadav P, Bandyopadhyay A, Chakraborty A, Sarkar K. Enhancement of anticancer activity and drug delivery of chitosan-curcumin nanoparticle via molecular docking and simulation analysis. *Carbohydr Polym*. 2018;182:188–198. doi:10.1016/j.carbpol.2017.10.102
15. Zhu JY, Yang X, Chen Y, et al. Curcumin suppresses lung cancer stem cells via inhibiting Wnt/beta-catenin and Sonic Hedgehog pathways. *Phytother Res*. 2017;31(4):680–688. doi:10.1002/ptr.5791
16. Mahran RI, Hagras MM, Sun D, Brenner DE. Bringing curcumin to the clinic in cancer prevention: a review of strategies to enhance bioavailability and efficacy. *AAPS J*. 2017;19(1):54–81. doi:10.1208/s12248-016-0003-2
17. Nabil G, Bhise K, Sau S, et al. Nano-engineered delivery systems for cancer imaging and therapy: recent advances, future direction and patent evaluation. *Drug Discov Today*. 2019;24(2):462–491. doi:10.1016/j.drudis.2018.08.009
18. Chen WL, Yang SD, Li F, et al. Tumor microenvironment-responsive micelles for pinpointed intracellular release of doxorubicin and enhanced anti-cancer efficiency. *Int J Pharm*. 2016;511(2):728–740. doi:10.1016/j.ijpharm.2016.07.060
19. Wu M, Cao Z, Zhao Y, et al. Novel self-assembled pH-responsive biomimetic nanocarriers for drug delivery. *Mater Sci Eng C Mater Biol Appl*. 2016;64:346–353. doi:10.1016/j.msec.2016.03.099
20. Yang X, Cai X, Yu A, Xi Y, Zhai G. Redox-sensitive self-assembled nanoparticles based on alpha-tocopherol succinate-modified heparin for intracellular delivery of paclitaxel. *J Colloid Interface Sci*. 2017;496:311–326. doi:10.1016/j.jcis.2017.02.033
21. Farshad MK, Soltani M, Souri M. Controlled anti-cancer drug release through advanced nano-drug delivery systems: static and dynamic targeting strategies. *J Control Release*. 2020;327:316–349. doi:10.1016/j.jconrel.2020.08.012
22. El-Hammadi MM, Delgado AV, Melguizo C, Prados JC, Arias JL. Folic acid-decorated and PEGylated PLGA nanoparticles for improving the antitumour activity of 5-fluorouracil. *Int J Pharm*. 2017;516(1–2):61–70. doi:10.1016/j.ijpharm.2016.11.012
23. Kurosawa Y, Furugen A, Nishimura A, et al. Evaluation of the effects of antiepileptic drugs on folic acid uptake by human placental choriocarcinoma cells. *Toxicol in Vitro*. 2018;48:104–110. doi:10.1016/j.tiv.2017.12.003
24. Sousa M, Luna LA, Fonseca LC, Giorgio S, Alves OL. Folic-acid-functionalized graphene oxide nanocarrier: synthetic approaches, characterization, drug delivery study, and antitumor screening. *ACS Appl Nano Mater*. 2018;1(2):922–932. doi:10.1021/acsanm.7b00324
25. Monteiro LOF, Fernandes RS, Oda CMR, et al. Paclitaxel-loaded folate-coated long circulating and pH-sensitive liposomes as a potential drug delivery system: a biodistribution study. *Biomed Pharmacother*. 2018;97:489–495. doi:10.1016/j.biopha.2017.10.135
26. Bakshi PR, Londhe VY. Widespread applications of host-guest interactive cyclodextrin functionalized polymer nanocomposites: its meta-analysis and review. *Carbohydr Polym*. 2020;242:116430. doi:10.1016/j.carbpol.2020.116430
27. Faezeh A, Sahar A, Majid G. Improve solubility of acetamidophenol from PEG and witepsol suppositories via formation of inclusion complex by β-cyclodextrin with a controlled release profile. *J Pharm Innov*. 2018;14(1):1–9. doi:10.1007/s12247-018-9328-y
28. Popat A, Karmakar S, Jambhrunkar S, Xu C, Yu C. Curcumin-cyclodextrin encapsulated chitosan nanoconjugates with enhanced solubility and cell cytotoxicity. *Colloids Surf B Biointerfaces*. 2014;117:520–527. doi:10.1016/j.colsurfb.2014.03.005
29. Hyun H, Lee S, Lim W, et al. Engineered beta-cyclodextrin-based carrier for targeted doxorubicin delivery in breast cancer therapy in vivo. *J Ind Eng Chem*. 2018;70. doi:10.1016/j.jiec.2018.09.052
30. Luong D, Kesharwani P, Alsaab HO, et al. Folic acid conjugated polymeric micelles loaded with a curcumin difluorinated analog for targeting cervical and ovarian cancers. *Colloids Surf B Biointerfaces*. 2017;157:490–502. doi:10.1016/j.colsurfb.2017.06.025
31. Guo F, Guo D, Zhang W, et al. Preparation of curcumin-loaded PCL-PEG-PCL triblock copolymeric nanoparticles by a microchannel technology. *Eur J Pharm Sci*. 2017;99:328–336. doi:10.1016/j.ejps.2017.01.001
32. Guo F, Wu J, Wu W, et al. PEGylated self-assembled enzyme-responsive nanoparticles for effective targeted therapy against lung tumors. *J Nanobiotechnology*. 2018;16(1):57. doi:10.1186/s12951-018-0384-8
33. Suh MS, Shen J, Kuhn LT, Burgess DJ. Layer-by-layer nanoparticle platform for cancer active targeting. *Int J Pharm*. 2017;517(1–2):58–66. doi:10.1016/j.ijpharm.2016.12.006

34. Liao J, Zheng H, Fei Z, et al. Tumor-targeting and pH-responsive nanoparticles from hyaluronic acid for the enhanced delivery of doxorubicin. *Int J Biol Macromol*. 2018;113:737–747. doi:10.1016/j.ijbiomac.2018.03.004

35. Jiang QY, Lai LH, Shen J, et al. Gene delivery to tumor cells by cationic polymeric nanovectors coupled to folic acid and the cell-penetrating peptide octaarginine. *Biomaterials*. 2011;32(29):7253–7262. doi:10.1016/j.biomaterials.2011.06.015